

Theory of critical enhancement of photorefractive beam coupling

E. V. Podivilov and B. I. Sturman

International Institute for Nonlinear Studies, Koptyug Avenue 1, 630090, Novosibirsk, Russia

M. V. Gorkunov, V. P. Kamenov, and K. H. Ringhofer

Department of Physics, University Osnabrueck, D-49069, Osnabrueck, Germany

(Received 31 October 2001; published 12 April 2002)

We develop the idea of critical enhancement of the photorefractive response near the threshold of parametric excitation of space-charge waves (the spatial subharmonics) taking into account the vectorial character of beam coupling and a fairly strong broadening of the nonlinear resonance owing to light absorption. The results of our calculations are a description of the measurable characteristics of critical enhancement and optimization of the experimental conditions for detection of anomalously high amplification gain factors in cubic $\text{Bi}_{12}\text{SiO}_{20}$ crystals.

DOI: 10.1103/PhysRevE.65.046623

PACS number(s): 42.65.Hw, 42.70.Nq

I. INTRODUCTION

Most of the known nonlinear effects in photorefractive media are caused by the optical photorefractive nonlinearity, whose main constituents are charge separation under light and diffraction on a corresponding index replica. Among these effects are spatial amplification, phase conjugation, optical oscillations, pattern formation, soliton propagation, and others [1–3]. The nonlinearity of the material equations for the light-induced space-charge field plays here a secondary role, if any.

The generation of spatial subharmonics in fast photorefractive materials—detected first in cubic $\text{Bi}_{12}\text{SiO}_{20}$ crystals [4–6] and found then [7–9] in the other representatives of the sillenite family ($\text{Bi}_{12}\text{TiO}_{20}$ and $\text{Bi}_{12}\text{GeO}_{20}$) and in the semiconductor CdTe—has been recognized as a fundamental phenomenon caused fully by the material nonlinearity. This conclusion is based not only on theoretical considerations [10–13] but also on firm experimental evidence [14,15].

It is well established nowadays (see [2,11,16,17] and references therein) that subharmonic generation during optical two-wave mixing is caused by parametric instability of the fundamental space-charge grating, recorded by two coherent light beams, against excitation of weakly damped space-charge waves (SCWs). The necessary precondition for this instability is either application of a dc electric field E_0 together with the introduction of a small frequency detuning Ω between the pump beams or application of a rapidly oscillating ac field. If \vec{K} is the fundamental grating vector (the difference between the light wave vectors) then the wave vector of the parametrically excited SCW is $\vec{K}/2$, its eigenfrequency is $\omega_{\vec{K}/2}$, and the condition for parametric resonance reads $\Omega = 2\omega_{\vec{K}/2}$.

The development of subharmonic theory based on the idea of parametric excitation of SCWs [18,19] has allowed an explanation of a number of distinctive features of the subharmonic generation [14,15,20,21]. The notion of space-charge waves has given new additional into the known mechanisms of dc and ac enhancement of the fundamental grating [2,3] by identifying the relevant enhancement factor

with the quality factor of the SCW, Q_K . Within the above development, the optical processes were expected to serve merely for visualization of SCWs by means of Bragg diffraction.

Recently, it was found [22] that joint action of the material and optical nonlinearities can result in qualitatively new optical effects having as a common root the critical enhancement of the photorefractive response. This critical enhancement is distinguished by the feasibility of making the photorefractive response (and the relevant optical effects) arbitrarily strong by approaching the subharmonic generation threshold controlled by the material nonlinearity. The main idea of this critical enhancement is to use the pliancy of the subharmonic grating (near the threshold of the instability) for its efficient excitation. Note that the optical scheme proposed in [22] is basically the same as that investigated earlier [23,24] in an attempt to explain the subharmonic generation by pure optical mechanisms. Omission of the terms relevant to the material nonlinearity in the initial equations did not allow Refs. [23,24] to demonstrate critical enhancement.

Unfortunately, the model considered in [22] is too illustrative; it does not include two important attributes of the photorefractive nonlinearity in cubic crystals expected to be appropriate for detection and utilization of critical enhancement. Correspondingly, it is not capable of describing the expected observable characteristics of this phenomenon and the optimization of the experimental conditions.

The first of the above mentioned attributes is attenuation of the total light intensity I_0 because of light absorption. Since the subharmonic eigenfrequency $\omega_{\vec{K}/2}$ is proportional to I_0 , the resonance condition $\Omega = 2\omega_{\vec{K}/2}$ can be satisfied only within a relatively thin layer of the crystal. Hence, the critical enhancement can deteriorate and the resonant optical characteristics are subjected to a nonuniform broadening [25,26]. The second attribute is the vectorial character of beam coupling in cubic photorefractive crystals [27,28]. In contrast to strongly anisotropic materials (like LiNbO_3), the polarizations of the interacting light waves change strongly because of the linear (optical activity and field-induced birefringence) and nonlinear (vectorial diffraction) optical effects.

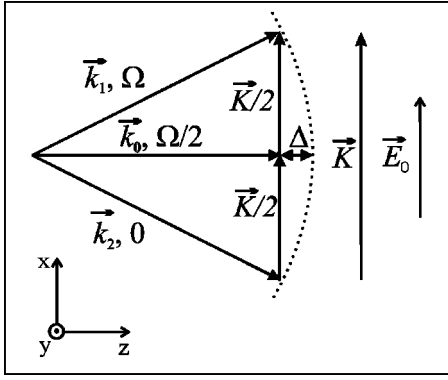


FIG. 1. Wave vector diagram for the critical enhancement. The grating vector $\vec{K} = \vec{k}_1 - \vec{k}_2$ is parallel to the applied field \vec{E}_0 ; the wave vector \vec{k}_0 is parallel to the propagation axis z .

The present paper aims for an extended analysis of the observable characteristics of critical enhancement by taking into account the above attributes. This includes formulation of a vectorial model of critical enhancement incorporating the effects of spatial inhomogeneity (Sec. II), an analytical treatment of this model (Sec. III), numerical characterization of the critical spatial amplification (Secs. IV and V), and discussion of experimental issues relevant to the detection of the effect under study (Sec. VI).

II. BASIC RELATIONS

A schematic diagram for critical enhancement which is not much different from that of [22] is presented in Fig. 1. Two pump waves with wave vectors \vec{k}_1 and \vec{k}_2 , frequency detuned by Ω , propagate symmetrically near the z axis in a cubic crystal appropriate for subharmonic generation. They produce a light intensity grating with the grating vector $\vec{K} = \vec{k}_1 - \vec{k}_2$ moving with velocity Ω/K in the x direction and also a corresponding grating of light-induced space charge. In addition to the pump waves, a weak central wave with wave vector \vec{k}_0 , detuned by $\Omega/2$, travels along the z axis. For convenience, we have set $|\vec{k}_0| = (k_{1,2})_z$; the small deficit of the wave vector Δ (the Bragg mismatch) will be treated within the envelope approximation. Thus we can say that the wave pairs 0,1 and 2,0 both contribute to the buildup of the subharmonic $K/2$ grating moving with the same velocity as the K grating. The last important element shown in the diagram is a dc electric field \vec{E}_0 applied in the x direction. This field facilitates charge separation and makes the space-charge waves weakly damped [11].

We assume now that $\Omega \approx 4\omega_K \equiv 2\omega_{K/2}$, where $\omega_K \propto I_0/KE_0$ is the frequency of the SCW with wave vector K and I_0 is the total pump intensity [11]. This means that we are not far from the parametric resonance for excitation of the subharmonic $K/2$, not far from the linear resonance for excitation of the subharmonic by the wave pairs 0,1 and 2,0, and far from the fundamental resonance (where $\Omega \approx \omega_K$). The pump intensity I_0 decreases with the propagation coordinate as $\exp(-\alpha z)$, where α is the light absorption coefficient.

Therefore $\omega_K = \omega_K(z)$ and the exact equality $\Omega = 4\omega_K$ cannot be satisfied in the whole crystal. To justify the above assumption of the proximity of the subharmonic resonance in the whole crystal, we have to restrict ourselves to the case of weak absorption, $\alpha d \ll 1$, where d is the crystal thickness. This inequality is not very restrictive for critical enhancement. In particular, it does not mean that we ignore the uniform broadening of the resonance. This effect can still be strong in our theory because the width of the resonance is considerably smaller than ω_K (see below).

We can now turn to the relations describing excitation of the space-charge field. Let e_K and $e_{K/2}$ be the envelopes of the space-charge field harmonics oscillating as $\exp[i(Kx - \Omega t)]$ and $\exp[i(Kx - \Omega t)/2]$, respectively, and $\vec{a}_0, \vec{a}_1, \vec{a}_2$ be the vectorial amplitudes of the light waves 0,1,2 normalized to $\sqrt{I_0}$ so that $|\vec{a}_1|^2 + |\vec{a}_2|^2 = 1$ within the undepleted pump approximation. Then, using the results of [11,18] and the equality $\Omega \approx 2\omega_{K/2}$, we can write down the following governing equation for the subharmonic amplitude $e_{K/2}$:

$$[\partial_t + \gamma_{K/2} + i\omega_{K/2} - i\Omega/2]e_{K/2} = i|\omega_{K/2}|(2e_K e_{K/2}^* - \vec{a}_0 \cdot \vec{a}_2^* - \vec{a}_1 \cdot \vec{a}_0^*). \quad (1)$$

The left-hand side shows the typical features of a forced wave oscillation. The first term on the right-hand side describes the parametric coupling between the fundamental amplitude e_K and $e_{K/2}$ caused by the material nonlinearity; it is responsible for the subharmonic generation. The last two terms account for the linear excitation of the subharmonic grating by the wave pairs 0,2 and 1,0. Note that the products $\vec{a}_0 \cdot \vec{a}_2^*$ and $\vec{a}_1 \cdot \vec{a}_0^*$ are nothing else than the half values of the light contrast induced by these pairs; they do not suffer from the linear light absorption. At the same time, the coefficients $\gamma_{K/2}$ and $\omega_{K/2}$ decrease as $\exp(-\alpha z)$ because of the intensity attenuation. Further, we express e_K through the pump contrast $m = 2\vec{a}_1 \cdot \vec{a}_2^*$. Since $\Omega \approx 4\omega_K$ is far from ω_K , the excitation of the fundamental grating is not resonant; using Eq. (23a) of [11] we have $e_K \approx m/6$. This relation holds true as long as the unit pump contrast and the fundamental amplitude e_K remain fairly small.

In steady state, resolving Eq. (1) with respect to $e_{K/2}$ and taking into account the pump intensity attenuation, we obtain

$$e_{K/2} = \frac{-i\tilde{Q}}{1 - \xi^2} \left[\vec{a}_0 \cdot \left(\vec{a}_2^* - \frac{im}{3}\tilde{Q}^* \vec{a}_1^* \right) + \vec{a}_0^* \cdot \left(\vec{a}_1 - \frac{im}{3}\tilde{Q}^* \vec{a}_2 \right) \right]. \quad (2)$$

Here $\tilde{Q} = [Q_{K/2}^{-1} + i\delta(z)]^{-1}$ is a complex resonant factor, $\delta = 1 - \Omega \exp(\alpha z)/4\omega_K(0)$ is the dimensionless distance to the subharmonic resonance [$|\delta(z)| \ll 1$], $\xi = |m\tilde{Q}|/3$ is the ratio of the pump contrast to its threshold value at a given frequency detuning δ , and the asterisk means complex conjugation. As seen from Eq. (2), the subharmonic amplitude $e_{K/2}$ tends to infinity when the threshold parameter ξ approaches

1. This feature, crucial for the effect under study, expresses mathematically the pliancy of the subharmonic grating mentioned in the Introduction. It is clearly seen from the expression for \tilde{Q} that the effect of frequency detuning becomes important for $|\delta| \approx Q_{K/2}^{-1} \ll 1$. At $\delta=0$ we have the minimum threshold value of the contrast, $m_{th}=3/Q_{K/2}$. The complex vectorial wave amplitudes $\vec{a}_{0,1,2}$ in Eq. (2) are generally slowly varying functions of the propagation coordinate z .

In our next step, we obtain the governing equation for the amplitude $\vec{a}_0(z)$. This amplitude is changing because of several factors. First, we should keep in mind the change owing to the Bragg mismatch Δ (see Fig. 1). Second, it changes because of optical activity and the optical anisotropy induced by the applied field. The above linear-optical effects change the direction of \vec{a}_0 . Third, and this is the most important, it changes because of diffraction of the pump beams from the subharmonic $K/2$ grating. This diffraction is also vectorial in cubic crystals, it is accompanied by a change of the polarization state. The progress made during recent years in description of vectorial coupling in cubic photorefractive crystals [26,28] allows us to describe the above processes in a general and compact form. Within the paraxial approximation, when only the x,y components of the light amplitudes are present, we have for \vec{a}_0

$$\begin{aligned} (\partial_z - i\Delta - i\vec{\kappa} \cdot \hat{\sigma}) \vec{a}_0 \\ = iE_0(\nu_0 + \vec{\nu} \cdot \hat{\sigma})(e_{K/2}^* \vec{a}_1 + e_{K/2} \vec{a}_2). \end{aligned} \quad (3)$$

Here $\vec{\kappa}=(\kappa_1, \rho, \kappa_3)$ (ρ is the rotatory power) and $\vec{\nu}=(\nu_1, 0, \nu_3)$ are certain known real three-dimensional (3D) vectors, ν_0 is a real known scalar parameter, and $\hat{\sigma}=(\hat{\sigma}_1, \hat{\sigma}_2, \hat{\sigma}_3)$ is the set of Hermitian sigma (Pauli) matrices [29]. The scalar products in Eq. (3) are understood in the conventional meaning, e.g., $\vec{\kappa} \cdot \hat{\sigma} \equiv (\kappa_1 \hat{\sigma}_1 + \kappa_2 \hat{\sigma}_2 + \kappa_3 \hat{\sigma}_3)$. The term $i\vec{\kappa} \cdot \hat{\sigma}$ describes the linear-optical properties while the terms of the right-hand side account for the above mentioned processes of vectorial diffraction. The absorption coefficient does not enter Eq. (3) because of our normalization of the light amplitudes to $\sqrt{I_0} \propto \exp(-\alpha z/2)$. The use of the σ matrices greatly simplifies operations with 2D vectorial amplitudes; see, e.g., [28,30].

The coefficients $\kappa_{1,3}$, $\nu_{1,3}$, and ν_0 , dependent on the electro-optical properties of the crystal, can be calculated for any particular optical configuration [28,31]. If we restrict ourselves to the $[1\bar{1}0]$ (or $[110]$) crystal cut, which corresponds to all known experiments on subharmonic generation, the components $\kappa_{1,3}$ can be presented in the form $\kappa_1 = qE_0 \sin \zeta$, $\kappa_3 = -0.5qE_0 \cos \zeta$, where ζ is the angle between the grating vector \vec{K} and the $[001]$ axis, $q = \pi n^3 r_{41} / \lambda$, n is the refractive index, and r_{41} is the electro-optic constant. The coefficients $\nu_{0,1,3}$ generally include not only the electro-optic but also elasto-optic contributions [32,33]; the latter are often of minor importance. With the elasto-optic contributions

omitted, we have $\nu_0 = 0.5q \cos \zeta$, $\nu_1 = q \sin \zeta$, and $\nu_3 = -0.5q \cos \zeta$.

The cases

$$\zeta = 0 \quad (\vec{K} \parallel \vec{E}_0 \parallel [001])$$

and

$$\zeta = \pi/2 \quad (\vec{K} \parallel \vec{E}_0 \perp [001])$$

correspond to the so-called longitudinal (L) and transverse (T) optical configurations. Most of the subharmonic experiments have been performed in the L geometry and only a few in the T configuration. Omission of the elasto-optic contributions is well justified for these cases. It is worth noting that the directions $[001]$ and $[00\bar{1}]$ cannot be distinguished in photorefractive experiments, nor can the positive and negative signs of r_{41} . However, by 180° rotations of the sample around the propagation axis we can always reverse the signs of $\kappa_{1,3}$ and $\nu_{0,1,3}$.

The coupling parameter ν_0 characterizes the scalar part of diffraction (with no polarization changes) whereas the vector $\vec{\nu}$ is responsible for the vectorial part of the interaction, generally changing the polarization state. The limit of scalar coupling corresponds to the equality $\vec{\nu} = \vec{0}$; it can never be realized in cubic photorefractive crystals. The opposite situation, $\nu_0 = 0$, where the vectorial character of the beam coupling is strongest, occurs in the T case.

The pump amplitudes $\vec{a}_{1,2}$ in Eq. (3) cannot be set equal to their input values because of the changes owing to the linear and nonlinear effects. The linear effects (optical activity and the field-induced anisotropy) are the same for them as for the central beam. As for the effect of beam coupling on $\vec{a}_{1,2}$, it can be neglected under fairly weak restrictions on the crystal thickness. The point is that coupling via the K grating (see Fig. 1), is weak because this grating is driven far from resonance ($\Omega - \omega_K \approx 3\omega_K \gg \gamma_K$). For any reasonable crystal parameters, the above accepted inequality $\alpha d \ll 1$ justifies omission of the relevant diffraction terms. As for the effect of pump depletion owing to diffraction from the subharmonic $K/2$, it can be made negligible by using a sufficiently weak input central beam. Under the assumptions made, the pump amplitudes $\vec{a}_{1,2}$ obey Eq. (3) with zero right-hand side, which can easily be solved [28].

By substituting $e_{K/2}$ given by Eq. (2) into Eq. (3), one can arrive at a closed equation for \vec{a}_0 . We make, however, one more step in the simplification of the initial equations by performing the unitary transformation

$$\begin{aligned} \vec{a}_{0,1,2} &= \exp(iz\vec{\kappa} \cdot \hat{\sigma}) \vec{b}_{0,1,2} \\ &= [\cos(\kappa z) + i\kappa^{-1}(\vec{\kappa} \cdot \hat{\sigma}) \sin(\kappa z)] \cdot \vec{b}_{0,1,2} \end{aligned} \quad (4)$$

from the amplitudes $\vec{a}_{0,1,2}$ to $\vec{b}_{0,1,2}$, where $\kappa = |\vec{\kappa}|$.

For the new pump amplitudes we have $\partial_z \vec{b}_{1,2} = 0$, i.e., $\vec{b}_{1,2}(z) = \vec{b}_{1,2}(0) = \vec{a}_{1,2}(0)$. In other words, these new pump amplitudes equal the input values of the old ones.

Transformation of the equation for \vec{a}_0 is somewhat more difficult because the operator $\vec{\nu} \cdot \hat{\sigma}$ on its right-hand side does not commute with $\vec{\kappa} \cdot \hat{\sigma}$. Using Eq. (2) for $e_{K/2}$, assuming that the input polarizations of the pump beams are the same, and measuring the phase of the central beam from the half sum of the input pump phases $(\Phi_1 + \Phi_2)/2$, we obtain finally

$$(\partial_z - i\Delta)\vec{b}_0 = -\frac{E_0}{1 - \xi^2}[(\vec{b}_0 \cdot \vec{e}_0^*)(\vec{Q}'W_0 - i\vec{Q}'' + im_0|\vec{Q}|\xi) + i(\vec{b}_0^* \cdot \vec{e}_0)(|\vec{Q}|\xi - m_0\vec{Q}'')](\nu_0 + \vec{h} \cdot \hat{\sigma})\vec{e}_0, \quad (5)$$

where $W_0 = |\vec{a}_1(0)|^2 - |\vec{a}_2(0)|^2$ is the relative intensity difference of the input pump beams (the pump difference), $m_0 = (1 - W_0^2)^{1/2}$ is the input pump contrast, \vec{e}_0 is the input unit polarization vector of the pump,

$$\begin{aligned} \vec{Q}' &= \text{Re}(\vec{Q}) = Q_{K/2}(1 + \delta^2 Q_{K/2}^2)^{-1}, \\ \vec{Q}'' &= \text{Im}(\vec{Q}) = -\delta Q_{K/2}^2(1 + \delta^2 Q_{K/2}^2)^{-1}, \end{aligned} \quad (6)$$

$$\vec{h} = \vec{\nu} - 2 \sin^2(\kappa z)[\vec{\nu} - \vec{n}(\vec{n} \cdot \vec{\nu})] + (\vec{n} \times \vec{\nu})\sin(2\kappa z),$$

$\xi = m_0|\vec{Q}|/3$, and $\vec{n} = \vec{\kappa}/\kappa$.

In this way, we got rid of the linear term $\vec{\kappa} \cdot \hat{\sigma}$ in Eq. (3) and explicitly expressed the coefficients in the right-hand side of the governing equation via the input parameters. The parameters δ and ξ are functions of z because of light absorption, and the dependence $\vec{h}(z)$ originates from optical activity. No input phases enter the coefficients of Eq. (5).

The use of the amplitudes \vec{b} instead of \vec{a} does not produce much trouble in calculating the observable characteristics because the unitary transformation (4) changes neither the wave intensities nor the scalar products, $|\vec{a}_0(z)|^2 = |\vec{b}_0(z)|^2$, $\vec{a}_1(z) \cdot \vec{a}_2^*(z) = \vec{b}_1(z) \cdot \vec{b}_2^*(z)$, etc. The input values of the \vec{b} amplitudes coincide with those of the amplitudes \vec{a} .

The most important element of Eq. (5) is, indeed, the presence of the critical factor $(1 - \xi^2)^{-1}$ on the right-hand side, which ensures an infinite growth of the rate of spatial amplification in the vicinity of the threshold of subharmonic generation. If we set $\xi = 0$ in Eq. (5), we return to the model of zero material nonlinearity. As in [22], the amplitude of the central beam \vec{a}_0 is coupled with the complex conjugate \vec{a}_0^* , which is the fingerprint of a parametric optical process. However, the vectorial character of the interaction and the effect of spatial inhomogeneity complicate the mathematical treatment of the problem.

It is useful to list and comment on the parameters affecting the critical enhancement. The variable experimental parameters can be separated into critical and noncritical. The critical variable parameters are those that enter the expression for $\xi = m_0 Q_{K/2}/3(1 + Q_{K/2}^2 \delta^2)^{1/2}$ with $\delta = 1 - [\Omega \exp(\alpha z)/4\omega_K(0)]$ and, therefore, define the proximity

of the singularity. First of all these are the frequency detuning Ω and the pump contrast m_0 (or W_0). The quality factor $Q_{K/2}$ depends on the applied field E_0 and the grating vector K . Some representative examples of this dependence are given in Sec. IV. The other (noncritical) variable experimental parameters are the polarizations of the input beams, the input phase of the central beam Φ_0 , and also the crystal thickness d . The mismatch Δ is also a noncritical parameter; it is expressed by K and the wavelength λ , $\Delta = \lambda K^2/16\pi n$. The material parameters relevant to the effect in question are $\epsilon\epsilon_0, n, r_{41}, \rho$, and also α, N_i , and $\mu\tau$. The last three parameters, which are most important, vary from sample to sample and furthermore the absorption coefficient α and the rotatory power ρ may depend strongly on the wavelength λ [3]. Some representative examples of the choice of the experimental parameters for $\text{Bi}_{12}\text{SiO}_{20}$ crystals are given in Sec. IV.

III. THE SIMPLIFIED VECTORIAL MODEL

It is important that for sufficiently thin crystals the effects of spatial inhomogeneity in Eq. (5) become negligible whereas the critical optical nonlinear effects remain quite strong. As seen from Eq. (6) for \vec{h} and the expression for δ , the spatial inhomogeneity becomes negligible when $\alpha d \ll Q_{K/2}^{-1} < 1/3$, $\rho d \ll 1$, and $qE_0 d \equiv \pi n^3 r_{41} E_0 d/\lambda \ll 1$. In this limit $\vec{h} = \vec{\nu}$, $\omega_K = \omega_K(0)$, and therefore $\delta = (\Omega - 4\omega_K)/4\omega_K$ do not depend on z , so that the parameters \vec{Q} and $\xi = m_0|\vec{Q}|/3$ [see Eqs. (6)], are also constant. The difference between the amplitudes $\vec{b}(z)$ and $\vec{a}(z)$ is likewise negligible in the limit of a thin crystal.

With spatially uniform coefficients, the vectorial governing equation (5) admits an analytical treatment. Multiplying it by \vec{e}_0^* and setting $(\vec{e}_0^* \cdot \vec{a}_0), (\vec{e}_0 \cdot \vec{a}_0^*) \propto \exp(\Gamma z)$, we obtain after simple algebraic calculations a quadratic equation for the rate of spatial amplification (the increment) Γ . Solution of this equation gives two branches of the increment,

$$\Gamma_{\pm} = f_1 \pm \sqrt{g^2 - f_2^2} \quad (7)$$

with

$$\begin{aligned} f_1 &= -\frac{\vec{\nu} E_0 \vec{Q}' W_0}{1 - \xi^2}, \\ f_2 &= \Delta - \frac{\vec{\nu} E_0}{1 - \xi^2}(m_0 \xi |\vec{Q}| - \vec{Q}''), \\ g &= -\frac{\vec{\nu} E_0}{1 - \xi^2}(\xi |\vec{Q}| - m_0 \vec{Q}''), \end{aligned} \quad (8)$$

where the real quantity $\vec{\nu} = \nu_0 + \vec{\nu} \cdot \vec{s}_0$ is an effective coupling constant and \vec{s}_0 is the Stokes vector with three real components [34] characterizing the input polarization state of the pump. For linear polarization these components are expressed by the input polarization angle φ_0 ; if it is measured

from the [001] axis, then $(s_0)_1 = \sin 2\varphi_0$, $(s_0)_2 = 0$, $(s_0)_3 = \cos 2\varphi_0$. For circular input pump polarization $(s_0)_{1,3} = 0$, $(s_0)_2 = \pm 1$.

Equations (7) and (8) are our generalization of the relevant expressions of the scalar model [22] to the vectorial case. They include the polarization and orientation dependences of the increment Γ and also its dependence on the frequency detuning Ω . Note that the increment Γ does not depend on the input polarization and phase of the central beam.

The quantities Γ_{\pm} are real for $g^2 \geq f_2^2$ and complex for $g^2 < f_2^2$ when the square root in Eq. (7) becomes imaginary. The inequality $g^2 < f_2^2$ is satisfied for a relatively large mismatch Δ , i.e., essentially for off-Bragg diffraction to the central beam. In what follows, we refer to the regions of variable parameters where $g^2 > f_2^2$ and $g^2 < f_2^2$ as the Bragg and off-Bragg regions, respectively. When approaching the singularity $\xi(\Omega, W_0) \rightarrow 1$, the square root always becomes positive, whereas the deficit Δ becomes unimportant and diffraction becomes Bragg-like.

Near the singularity ($0 < 1 - \xi \ll 1$) Eq. (7) is strongly simplified. One of the branches, which is of our main interest, tends to $\pm \infty$ when $\xi \rightarrow 1$, and the second branch remains finite. The positive value of the singular branch corresponds to the inequality $\bar{\nu} E_0 W_0 < 0$; in this case

$$\Gamma_+ \approx - \frac{3E_0 W_0 (\nu_0 + \vec{\nu} \cdot \vec{s}_0)}{m_0 [(1 + \delta^2 Q_{K/2}^2)^{1/2} - (Q_{K/2} m_0 / 3)]}. \quad (9)$$

In turn, the inequality $\bar{\nu} W_0 E_0 < 0$ can always be satisfied by changing either the sign of W_0 or the sign of $\bar{\nu}$; the last one can be inverted by a 180° rotation of the sample around the z axis. Note that inverting E_0 changes the sign of ω_K . The cases $\bar{\nu} E_0 < 0, W_0 > 0$ and $\bar{\nu} E_0 > 0, W_0 < 0$ are not equivalent. The second choice is best for critical enhancement because the nonlinear correction to the wave number k_0 is negative here; it compensates for the mismatch Δ and facilitates Bragg diffraction. In experiment, the sign of W_0 can be optimized by reversing the pump ratio.

The absolute value of the effective coupling constant $\bar{\nu} = \nu_0 + \vec{\nu} \cdot \vec{s}_0$ depends on the input pump polarization and also on the choice of the optical configuration. To characterize the polarization dependence, we mention that the Hermitian operator $\vec{\nu} \cdot \hat{\sigma}$ possesses two mutually orthogonal real unit eigenvectors \vec{e}_{\pm} such that $(\vec{\nu} \cdot \hat{\sigma}) \vec{e}_{\pm} = \pm \nu \vec{e}_{\pm}$. If we set the pump polarization vector \vec{e}_0 equal to \vec{e}_{\pm} then $\bar{\nu} = \nu_0 \pm \nu$. Correspondingly, the maximum and minimum values of $|\bar{\nu}|$ are $|\nu_0| + |\nu|$ and $|\nu_0| - |\nu|$. For both the longitudinal and transverse optical configurations $|\bar{\nu}|_{max}$ equals the same value $|q| = |\pi n^3 r_{41} / \lambda|$. The optimum pump polarization is linear; for the longitudinal geometry the optimum polarization angle φ_p , measured from [001], is 90° and for the transverse case it is $\pm 45^\circ$. A circular pump polarization turns the scalar product $\vec{\nu} \cdot \vec{s}_0$ to zero.

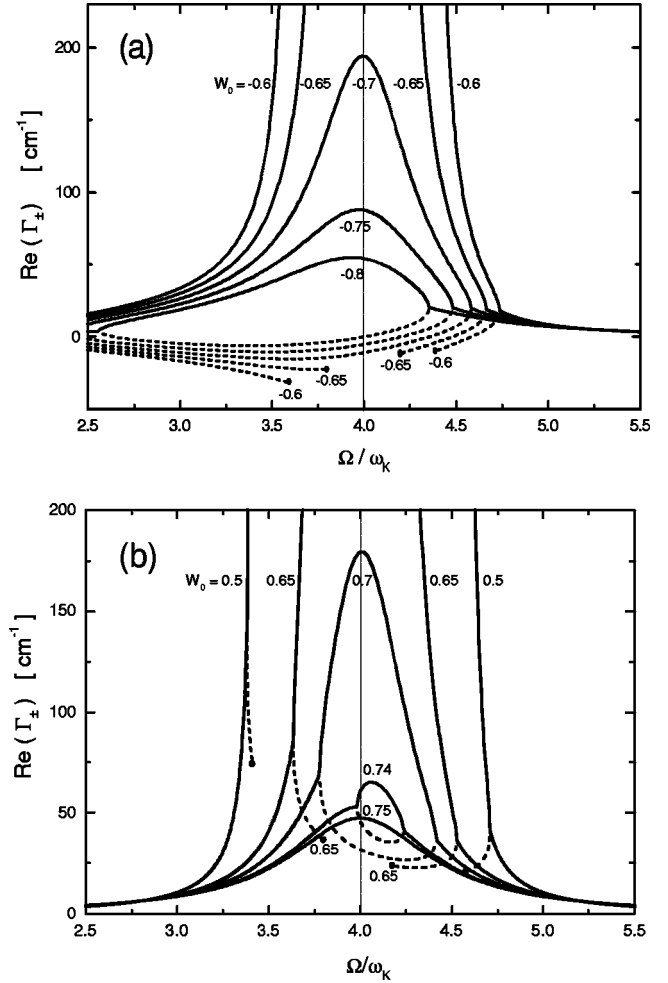


FIG. 2. Dependence of $\text{Re}(\Gamma_{\pm})$ on the frequency detuning for $Q_{K/2} = 4$, $|\bar{\nu} E_0| = 3.5 \text{ cm}^{-1}$, and $\Delta = 20.7 \text{ cm}^{-1}$ for several values of the pump difference W_0 . The cases (a) and (b) correspond to the combinations $\bar{\nu} > 0, W_0 < 0$ and $\bar{\nu} < 0, W_0 > 0$, respectively. The dashed lines are plotted for the lower branch of the increment, $\Gamma_-(\Omega)$; the dots mark the points of singularity for $\Gamma_+(\Omega)$.

The main critical parameters entering Eq. (7) are the detuning Ω and the pump difference W_0 . Figure 2(a) shows the functions $\text{Re}[\Gamma_{\pm}(\Omega)]$ for $Q_{K/2} = 4$, $\Delta = 20.7 \text{ cm}^{-1}$, $\bar{\nu} E_0 = 3.4 \text{ cm}^{-1}$ (see the next section for more details), and several negative values of W_0 . Each of the dependences $\Gamma_{\pm}(\Omega)$ generally possesses two bifurcation points where $\sqrt{g^2 - f_2^2} = 0$. Before the bifurcation, i.e., in the off-Bragg regions, the roots Γ_+ and Γ_- are complex conjugate to each other and the values of $\text{Re}[\Gamma_+(\Omega)] = \text{Re}[\Gamma_-(\Omega)]$ are rather small. After the bifurcation, i.e., in the Bragg regions, the increments are real and the upper branch $\Gamma_+(\Omega)$ goes up rapidly with decreasing distance to the resonance $|\Omega - 4\omega_K|$.

Below threshold, $|W_0| > 0.66$ ($m_0 < 0.75$), the whole resonant region is available for our theory. The dependence $\Gamma_+(\Omega)$ is characterized here by an asymmetric and fairly wide peak centered at $4\omega_K$. Its height tends to infinity for $|W_0| \rightarrow 0.66$. For $m_0 > m_{th} = 0.75$ our theory is applicable only to the frequency wings, $3|\delta| > (m_0^2 - m_{th}^2)^{1/2}$; for smaller

distances the central beam appears without any seed. When approaching the boundary of the permitted frequency region, the increment $\Gamma_+(\Omega)$ grows infinitely. The branch $\Gamma_-(\Omega)$, shown by dotted lines, does not exhibit any singularity. The end of each dotted line corresponds to the singular point for the corresponding solid line. Without the critical enhancement, the maximum expected value of Γ does not exceed $Q_{K/2}|\bar{\nu}E_0| \approx 13 \text{ cm}^{-1}$.

Figure 2(b) shows the dependences $\text{Re}[\Gamma_{\pm}(\Omega)]$ for $\bar{\nu}E_0 = -3.4 \text{ cm}^{-1}$ and $W_0 > 0$. This case is not the best for Bragg diffraction. With the other parameters remaining the same, the value of $\text{Re}[\Gamma_+(\Omega, |W_0|)]$ is smaller here than the one in the previous case, the bifurcation points are closer to $4\omega_K$, and they correspond to larger values of the increment. The singular behavior remains, however, essentially the same.

With our analysis of the properties of the increment completed, it is useful to present an explicit expression for the projection $a_0 = \vec{e}_0^* \cdot \vec{a}_0$. Within the simplified model we have

$$a_0 = -\frac{1}{2\sqrt{g^2 - f_2^2}} \{ [a_0(0)(f - \Gamma_+) - i g a_0^*(0)] e^{\Gamma_+ z} - [a_0(0)(f - \Gamma_-) - i g a_0^*(0)] e^{\Gamma_- z} \}, \quad (10)$$

where $f = f_1 - i f_2$. In the case when the increments are real and $\exp[(\Gamma_+ - \Gamma_-)z] \gg 1$ (which is always attainable in the Bragg region), the term proportional to $\exp(\Gamma_+ z)$ dominates in Eq. (10). When approaching the off-Bragg region of Ω (see Fig. 2), the second exponent becomes important. As a result, the dependence $|a_0(\Omega)|^2$ experiences some jerks near the bifurcation points (see also Sec. V; the spatial growth here is not always monotonic and is not exponential).

The preexponential factors in Eq. (10) depend periodically (with a period of π) on the phase of the central beam Φ_0 . Their effect on $|\vec{a}_0|$ is very weak for the critical enhancement except in the close vicinity of the point Φ_0^+ where the factor before the exponent $\exp(\Gamma_+ z)$ turns to zero. This value of the phase, unwanted for amplification, is given by $2\Phi_0^+ = \pi + \Phi_1 + \Phi_2 + \arctan(\sqrt{g^2 - f_2^2}/f_2)$, where $\Phi_{1,2}$ are the input values of the phase for the pump beams 1,2. The coincidence of the input phase Φ_0 with the unwanted value Φ_0^+ can only be occasional.

Fluctuations of the input phases can wash out the dip in the dependence of the amplification factor on Φ_0 .

Lastly, we note that with the optimized pump polarization vector \vec{e}_0 only the projection of the amplitude \vec{a}_0 to \vec{e}_0 is subject to spatial amplification. The optimum input polarization of the central beam here is indeed the same as the pump polarization.

IV. MODEL CHARACTERISTICS OF $\text{Bi}_{12}\text{SiO}_{20}$ CRYSTALS

Cubic crystals of $\text{Bi}_{12}\text{SiO}_{20}$ (BSO) belonging to the point group 23 are perhaps the best choice for detection of the critical enhancement. Most of the subharmonic experiments, including the most precise ones [14,15,35,36], have been

performed with this material. Its main optical and photorefractive characteristics are well described in the literature [3,27]. Below we specify the relevant material characteristics, estimate the corresponding model parameters, analyze the applicability of the simplified vectorial model, and consider the range of variable experimental parameters feasible for detection of the critical enhancement.

As representative material parameters of BSO crystals we choose $\epsilon\epsilon_0 = 56$, $n = 2.6$, $\rho = 38.6 \text{ deg/mm} \approx 6.74 \text{ cm}^{-1}$, $r_{41} = 4.51 \text{ pm/V}$, $N_r = 10^{16} \text{ cm}^{-3}$, $\mu\tau = (1-6) \times 10^{-7} \text{ cm}^2/\text{V}$, and $\alpha = 1-2 \text{ cm}^{-1}$. The pump wavelength λ we set equal to 514 nm; this value is most typical of subharmonic experiments.

With these figures we estimate $|q| \equiv \pi n^3 |r_{41}| / \lambda \approx 4.85 \times 10^{-4} \text{ V}^{-1}$. Correspondingly, the rate of spatial change of the light amplitudes owing to the field-induced anisotropy $\approx qE_0$ (measured in cm^{-1}) is estimated as $\approx 0.48E_0 \text{ kV/cm}$. It becomes comparable with or larger than the rate of rotation of the polarization plane owing to optical activity ($\approx 6.74 \text{ cm}^{-1}$) only for $E_0 \geq 15 \text{ kV/cm}$. Therefore the condition $\kappa d \ll 1$ is equivalent to the restriction on the crystal thickness $d \leq 1.5 \text{ mm}$ for the field $E_0 \leq 15 \text{ kV/cm}$.

In the longitudinal geometry we have for the parameters $\nu_{0,1,3}$, characterizing the optical nonlinearity $\nu_0 = q/2$, $\nu_1 = 0$, and $\nu_3 = -q/2$. For linear input pump polarization we obtain here $\bar{\nu} = 0.5q(1 - \cos 2\varphi_0)$; the value $|\bar{\nu}|_{\max} = |q|$ corresponds to the polarization angle $\varphi_0 = \pi/2$, i.e., $\vec{a}_{1,2}(0) \perp [001]$. In the transverse geometry the scalar part of the beam coupling is absent, $\nu_0 = 0$; furthermore, $\nu_1 \approx q$ and $\nu_3 = 0$. Here we have $\bar{\nu} \approx q \sin 2\varphi_0$ for linearly polarized pump beams so that the value $\bar{\nu} \approx |q|$ corresponds to $\varphi_0 = \pm \pi/4$. Note that we have deliberately used the sign \approx in the T case. The point is that the elasto-optic contributions to ν_1 make it slightly (by $\approx 13\%$) larger than q (see [28] and references therein). With this accuracy, the value $|\bar{\nu}|_{\max} = |q|$ is the same for the L and T cases, so that the data of Fig. 2 are applicable to both these optical configurations, and the chosen value of $|q|$ is a good estimate for BSO crystals.

Next we need to characterize the subharmonic quality factor $Q_{K/2}$. Figure 3 shows the dependence $Q_{K/2}$ on E_0 and the half pump angle (in air) θ_p for two representative values of the $\mu\tau$ product. One sees that the condition $Q_{K/2} > 3$ is satisfied within a fairly wide range of E_0 and θ_p . The larger is $\mu\tau$, the wider is this region and the higher is the attainable value of the quality factor. For $E_0 \leq 1.5-2 \text{ kV/cm}$, where $Q_{K/2} < 3$, subharmonic generation is not expected. At the same time, increasing E_0 above 7-8 kV/cm gives no real gain for the quality factor. For $\mu\tau \leq 10^{-7} \text{ cm}^2/\text{V}$ subharmonic generation becomes impossible. For the same value of $Q_{K/2}$ the deficit $\Delta = \lambda K^2 / 16\pi n$ can acquire two different values; the smaller of them is expected to be preferable for critical enhancement. In what follows we use the value $E_0 = 7 \text{ kV/cm}$ in our numerical calculations.

If we take $\alpha = 1-2 \text{ cm}^{-1}$ and $Q_{K/2} = 5$, the inequality $\alpha d \ll Q_{K/2}^{-1}$ gives $d \ll 1-2 \text{ mm}$, which is not far from the restriction imposed by optical activity. In this way, for samples considerably thinner than 1 mm, the simplified vectorial

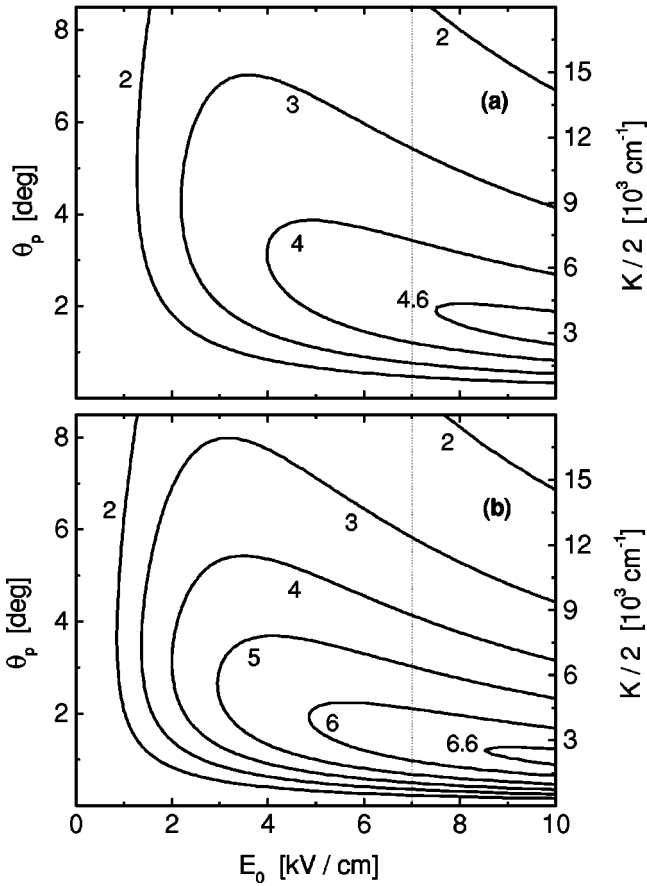


FIG. 3. Contour plots $Q_{K/2} = \text{const}$ on the K, E_0 plane for $\epsilon_0 = 56$ and $N = 10^{16} \text{ cm}^{-3}$; the cases (a) and (b) correspond to $\mu\tau = 3 \times 10^{-7}$ and $6 \times 10^{-7} \text{ cm}^2/\text{V}$, respectively.

model is justified, whereas for the thickness d considerably larger than 1 mm the negative effects of optical activity and the light absorption are expected to be strong.

In estimating an optimum crystal thickness for experiments regarding critical enhancement, it is necessary to keep in mind that the use of crystals considerably thinner than 1 mm makes it somewhat difficult to apply an electric field sufficient to achieve $Q_{K/2} \geq 3$. This brings us to the conclusion that $d \approx 1 \text{ mm}$ should be the best choice for experiment. The last argument in favor of this choice is the assertion that the noncritical mechanisms of spatial amplification remain fairly weak for $d \approx 1 \text{ mm}$ and cannot be a reason for misinterpretation of the experimental data. Any strong amplification effect can unambiguously be referred here to the critical enhancement.

The simplified vectorial model is not expected to be reliable for $d \approx 1 \text{ mm}$; it has to be supplemented by numerical calculations on the basis of Eqs. (5) and (6).

V. MODELING OF CRITICAL ENHANCEMENT IN BSO CRYSTALS

The dependence of the detuning δ upon z tends to deteriorate the resonance and to make the spatial profile of $|\vec{b}_0|$ nonexponential, but this dependence does not affect the di-

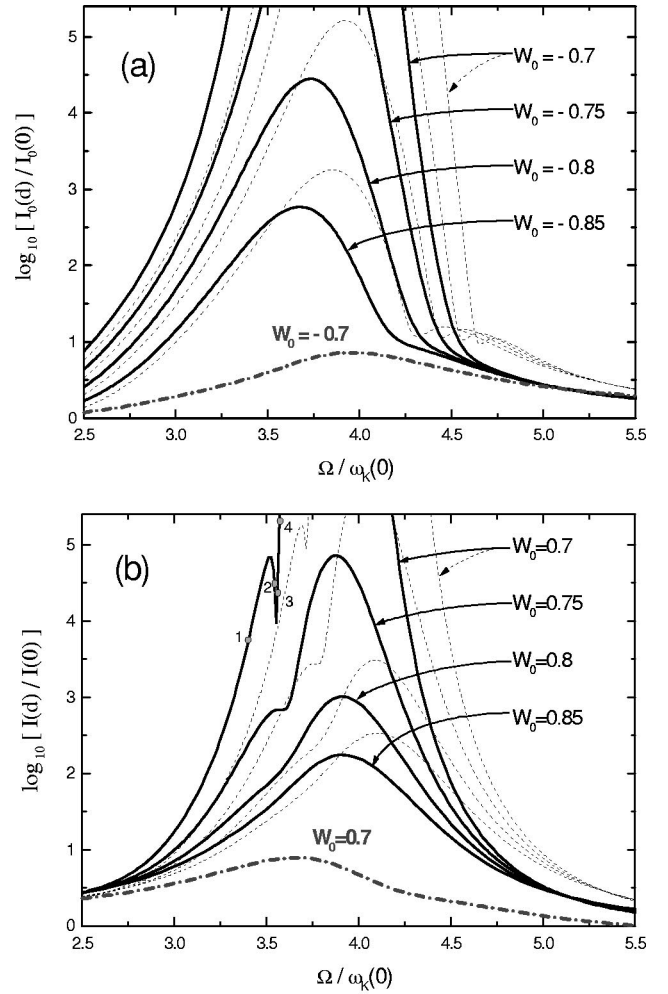


FIG. 4. Dependence of the gain factor $G = \log_{10}[|\vec{a}_0(d)|^2/|\vec{a}_0(0)|^2]$ on Ω for $d = 1 \text{ mm}$, $\theta_p = 1.2^\circ$, $Q_{K/2} = 4$, and other accepted parameters of BSO crystals. The cases (a) and (b) refer to the combinations $\bar{\nu} > 0, W_0 < 0$ and $\bar{\nu} < 0, W_0 > 0$, respectively. The solid lines are plotted on the basis of Eq. (5) and the dashed ones correspond to the simplified model. For all these graphs we have $m_0 < m_{th}$. The two dot-dashed gray lines in the cases (a) and (b) were obtained without taking account of the material nonlinearity.

rection of the vector $\vec{b}_0(z)$. However, the dependence of the vector \vec{h} upon z [which is mostly due to optical activity; see Eq. (6)] also changes the direction of $\vec{b}_0(z)$. In this way, the vectorial problem under study can by no means be reduced to a scalar one beyond the framework of the simplified model. Numerical simulation is here the main tool for a quantitative characterization of the critical enhancement. Below we shall see the difference between the simplified and exact solutions for critical enhancement in BSO crystals.

We start from an analysis of the gain factor $G = \log_{10}[|\vec{b}_0(d)|^2/|\vec{b}_0(0)|^2] \equiv \log_{10}[|\vec{a}_0(d)|^2/|\vec{a}_0(0)|^2]$. The solid lines in Fig. 4 show the dependence $G(\Omega)$ for the longitudinal geometry ($\vec{K} \parallel \vec{E}_0 \parallel [001]$), $d = 1 \text{ mm}$, $\alpha = 1 \text{ cm}^{-1}$, $Q_{K/2} = 4$, $E_0 = 7 \text{ kV/cm}$, $\Delta = 20.7 \text{ cm}^{-1}$ ($\theta_p \approx 1.2^\circ$), $\mu\tau = 3 \times 10^{-7} \text{ cm}^2/\text{V}$, and several representative

values of the pump intensity difference W_0 . All the input polarization vectors are chosen to be perpendicular to $[001]$ which is optimum for the simplified model. The subfigures (a) and (b) correspond to the cases $q > 0, W_0 < 0$ and $q < 0, W_0 > 0$; the first case is expected to be preferable for Bragg diffraction. The dashed lines exhibit the results obtained within the simplified model and the two dot-dashed curves show the dependence $G(\Omega)$ for $W_0 = \pm 0.7$ with the material nonlinear terms omitted.

One sees from Fig. 4 that the light absorption and optical activity make the critical spatial amplification noticeably weaker but they do not suppress it. As expected, the amplification remains stronger in the case (a) ($q > 0, W_0 < 0$). Below the threshold ($|W_0| = \sqrt{1 - m_0^2} > 0.66$) it is characterized by a frequency peak growing dramatically with increasing m_0 . It is remarkable that numerically high values of the gain are obtained already with the contrast m_0 considerably lower than $m_{th} = 0.75$. For example, we have almost three orders of magnitude amplification for $m_0/m_{th} \approx 0.7$ ($|W_0| = 0.85$) in Fig. 4(a) and more than two orders of magnitude in Fig. 4(b). Above threshold ($m_0 > 3/4$ or $|W_0| < 0.66$) our theory is applicable only to the frequency wings of the peak; compare with the data presented in Fig. 2. We do not show the corresponding wings to avoid overflow of the drawings.

The positions of the frequency maxima in Fig. 4 are shifted toward zero as compared to those found within the simplified model. This shift is fully due to light absorption (see also below). Some jerks in the frequency dependences of the gain factor [see, e.g., the two upper left wings in Fig. 4(b)] originate from bifurcation of the function $\Gamma(\Omega)$ (compare Fig. 2). In other words, each such jerk is a fingerprint of the transition between off-Bragg and Bragg regimes of diffraction. The effects of spatial inhomogeneity usually to smooth out the jerks [as in Fig. 4(a)] but sometimes they make them even more pronounced.

The regularities shown in Fig. 4 for the L geometry are essentially the same for the T case if the 90° value of the polarization angle φ_0 is replaced by a $\pm 45^\circ$ value. The only perceptible difference is a $\approx 13\%$ increase of the peak amplitudes because of the above mentioned elasto-optic contribution to ν_1 .

Increasing quality factor $Q_{K/2}$ lifts up the resonance curves and makes the resonance narrower and more strongly affected by the spatial inhomogeneity. The solid lines 1, 2, 3, and 4 in Fig. 5 exhibit the dependence $G(\Omega)$ for the L -configuration, $d = 1$ mm, $Q_{K/2} = 6$, $W_0 = -0.95$ ($m_0 \approx 0.31$), and four different values of the light absorption coefficient. The other relevant parameters correspond to Fig. 2(b). The dashed peak is plotted for the simplified model, $\alpha = \rho = 0$. The line 1 ($\alpha = 0$) shows that optical activity noticeably decreases the amplitude but does not change the peak profile; the resonant value of Ω and the shoulder on the right wing are essentially the same as for the dashed line. Increasing α shifts the peak toward zero, decreases its amplitude, increases the width, and washes out the shoulder. Note that $m_0/m_{th} \approx 0.625$ for the chosen parameters, i.e., we stay rather far from the singularity.

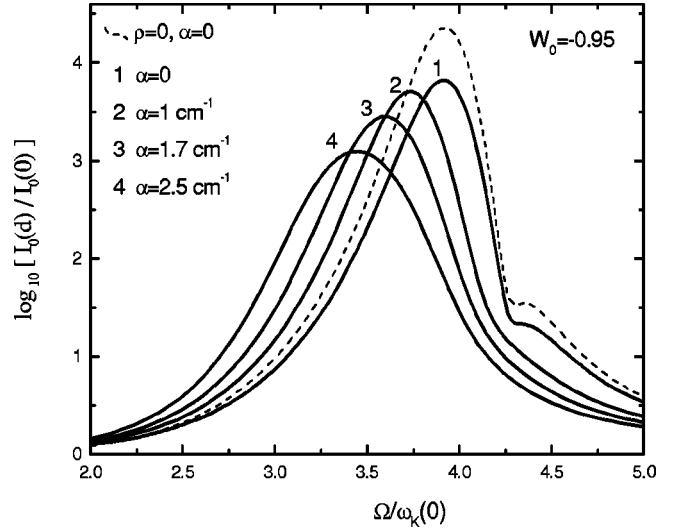


FIG. 5. Gain factor G versus Ω for $\mu\tau = 6 \times 10^{-7}$ cm²/V, $\theta_p \approx 1^\circ$, $\Delta \approx 13.7$ cm⁻¹ [see Fig. 2(a)], and $\varphi_0 = 90^\circ$. The curves 1, 2, 3, and 4 correspond to $\alpha = 0, 1, 1.7,$ and 2.5 cm⁻¹, respectively.

Next we consider the dependence of the gain factor on the propagation coordinate z . Within the simplified model this dependence is almost linear in the Bragg region when $\exp[(\Gamma_+ - \Gamma_-)z] \gg 1$. In our analysis we extend the propagation distance to $d = 2$ mm. The dependences $G(z)$ in Fig. 6 are plotted for the T configuration, $\varphi_0 = 45^\circ$, and five representative combinations of Ω and W_0 . The other parameters are the same as for Fig. 4(a). The curves 1, 2, and 3 refer to the left wing, the center, and the right wing of the frequency peak for $W_0 = -0.8$ which is quite similar to the corresponding peak of Fig. 4(a). The curves 4 and 5 refer to the left and right wings of a bigger peak (with $W_0 = -0.7$).

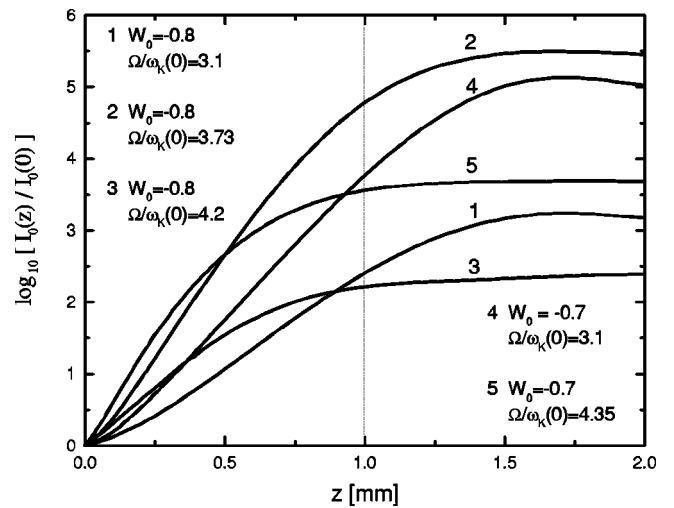


FIG. 6. Dependence $G(z)$ for the transverse geometry and $\varphi_0 = 45^\circ$. The curves are plotted for the following combinations of W_0 and $\Omega/\omega_K(0)$: 1 ($-0.8, 3.1$), 2 ($-0.8, 3.74$), 3 ($-0.7, 4.2$), 4 ($-0.7, 3.1$), and 5 ($-0.7, 4.35$). The other parameters are the same as for Fig. 4(a).

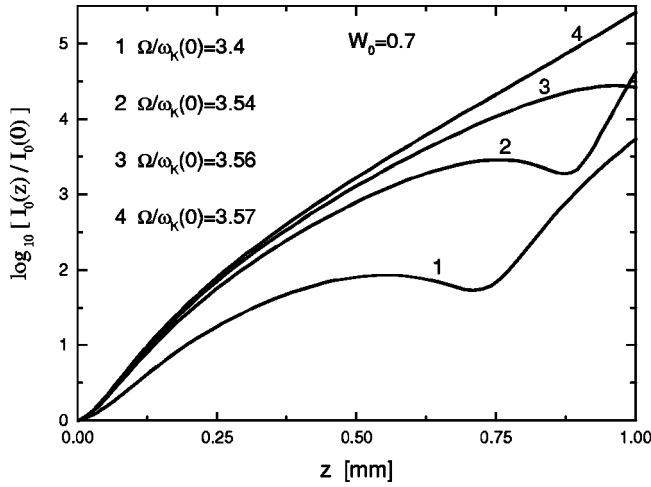


FIG. 7. Spatial dependence of the gain factor for the points 1, 2, 3, and 4 in Fig. 4(b).

For $z \lesssim 1$ mm the dependences $G(z)$ are not very different from those prescribed by the simplified model, although the tendency to saturation (caused mostly by the light absorption) is clearly seen for curves 3 and 5 representing the right wings. Optical activity here decreases the gain factor by no more than 20%. The extension of the propagation distance up to 2 mm leads to a strong saturation of the spatial growth. This saturation is predominantly due to optical activity. In a slightly relaxed form, this saturation is also present in the L case. A smaller negative effect of optical activity is caused here by the occurrence of the isotropic part of the beam coupling characterized by the scalar parameter ν_0 . The effect of saturation indeed leads to strong distortions of the frequency peaks of $G(\Omega)$ for $d \gtrsim 2$ mm.

Some peculiarities in the coordinate dependence of the gain factor can occur in the case $\bar{\nu} < 0, W_0 > 0$ where bifurcation of the dependence $\Gamma(\Omega)$ occurs at rather high values of the increment [see Fig. 2(b)]. Figure 7 shows the dependence $\Gamma(z)$ for four points marked in Fig. 4(b). In the off-

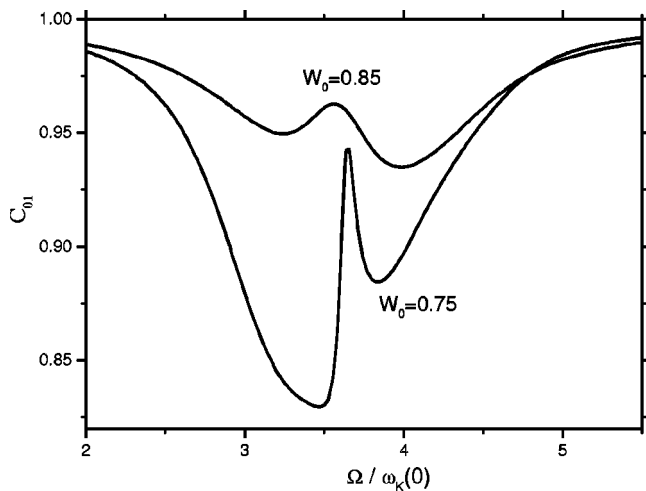


FIG. 8. Dependence of the degree of the polarization changes for the central beam, C_{01} , on Ω for the curves of Fig. 4(b) plotted for $W_0 = 0.85$ and 0.75 .

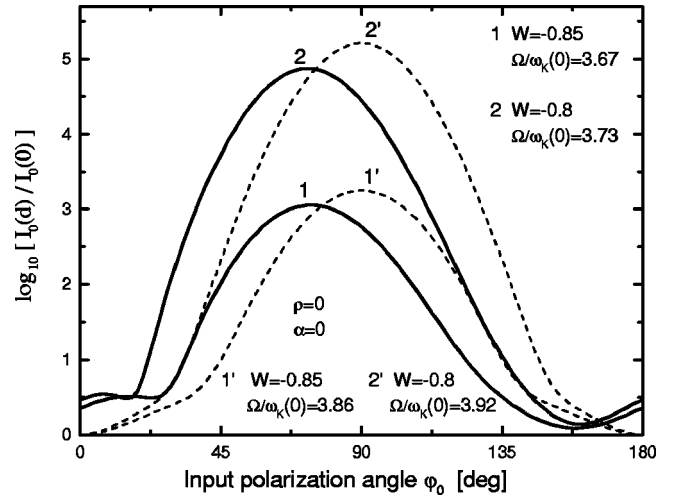


FIG. 9. Dependence $G(\varphi_0)$ for $d = 1$ mm in the L geometry. The graphs 1 and 2 are plotted for the peak values of $G(\Omega)$ in Fig. 4(a) corresponding to $W_0 = -0.85$ and -0.8 , respectively, and the curves 1' and 2' refer to the same peak values obtained within the simplified model.

Bragg region (points 1 and 2) the spatial dependence becomes nonmonotonic in contrast to the Bragg region (points 3 and 4).

In contrast to the simplified model, the output polarization state of the central beam is different from that of the pump beams because of the changing direction of $\vec{h}(z)$. To characterize this difference, we have calculated the parameter $C_{01} = |\vec{b}_0(d) \cdot \vec{b}_1^*(d)| / |\vec{b}_0(d)| |\vec{b}_1(d)|$, which can be considered as the cosine of the angle between the complex vectors \vec{b}_0 and \vec{b}_1 (\vec{a}_0 and \vec{a}_1). For identical and mutually orthogonal polarizations it equals 1 and 0, respectively. For the solid lines in Fig. 4 we have found that the value of C_{01} ranges, depending on Ω and W_0 , between 1 and 0.8. In other words, at the output the polarization of the central beam is not much different from the pump polarization. At the same time, the jerks of $G(\Omega)$ in Fig. 4 are accompanied by even sharper jerks in $C_{01}(\Omega)$. These are due to the effect of optical activity but not of light absorption. Two representative examples of the frequency dependence of C_{01} are shown in Fig. 8. With increasing gain factor G the values of C_{01} tend to decrease, i.e., the polarization changes become more pronounced.

Lastly, we consider the effect of the input polarization on the critical enhancement. The solid lines 1 and 2 in Fig. 9 show the dependence of the gain factor on the polarization angle φ_0 (the same for all beams) for two peak values of $G(\Omega)$ in Fig. 4(a). The corresponding dotted lines 1' and 2' illustrate the same polarization dependence within the simplified model. In the last case, the optimum angle φ_0 is indeed 90° . For the solid lines, the maximum is shifted to $\approx 74^\circ$ owing to the effect of optical activity. A similar result occurs for nonresonant values of the frequency detuning. Increasing crystal thickness makes this shift more pronounced.

VI. DISCUSSION

In our opinion, the analytical and numerical results presented give an extensive view of the expected characteristics

of the critical enhancement and allow us to give quite definite recommendations for the detection of this phenomenon in BSO crystals.

Most of the BSO samples for which subharmonic generation has been reported seem to be excessively thick for detection and investigation of the critical enhancement. The optimum thickness d is expected to be around 1 mm. The negative effects of light absorption and optical activity are moderate or small here; the competitive nonlinear optical effects are rather weak, whereas the effect under study is strong and controllable.

Reduction of the thickness of the sample implies shrinking of its transverse dimensions. Such a miniaturization of the sample facilitates application of a proper dc field (5–8 kV/cm for BSO crystals) and additionally allows the pump intensity to be increased to make the crystal response time shorter. Both these features are valuable for applications.

As our calculations show, operation below the subharmonic generation threshold $m_0 < m_{th} = 3/Q_{K/2}$ offers clear advantages for studies of the critical amplification. The whole frequency range is allowable here for measurements. By scanning the Ω dependence of the gain factor G , one can expect to see a dramatic increase of its peak value with the contrast m_0 incrementally approaching m_{th} from below.

The value of m_{th} can be optimized by varying the pump half angle θ_p within the range of 1° – 4° for $E_0 = 5$ – 8 kV/cm. To choose the optimum signs of the coupling constant $\bar{\nu}$ and the pump difference W_0 , one can make a 180° rotation of the sample around the propagation axis and reverse the input pump ratio $I_1(0)/I_2(0)$. For the transverse geometry the adjustment of the sign of $\bar{\nu}$ can also be performed by a 90° rotation of the input polarization plane for the pump beams.

To distinguish the critical enhancement from the usual two-wave coupling amplification, one can block the weakest pump beam. Strong drops in the gain will prove unambiguously an anomalous strength of the initial effect and the prime role of coupling of the subharmonic $K/2$ to the fundamental grating formed by the pump beams.

Since operation below threshold is preferable for critical enhancement experiments, it is not necessary to attain values of the quality factor $Q_{K/2}$ substantially larger than the minimum value of 3. This means, in turn, that the necessary restriction on the material parameters $\mu\tau$ and N_i is rather liberal, $N\mu\tau \geq 36\epsilon\epsilon_0/e$. For crystals of the sillenite family, BSO, $\text{Bi}_{12}\text{TiO}_{20}$, and $\text{Bi}_{12}\text{GeO}_{20}$, this gives roughly $\mu\tau \geq 10^{-7}$ cm²/V, which is certainly within the range of variation of the mobility-lifetime product.

The choice of the optical configuration is not really im-

portant for thin crystals; the L and T geometries are expected to give similar results for the critical enhancement. In the L geometry the negative effect of optical activity is somewhat weaker than in the T case. On the other hand, the T configuration allows one to test the sample for subharmonic generation in the absence of optical coupling [14,15].

The vectorial character of beam coupling in cubic crystals gives an additional handle to verify the properties of critical enhancement. The optimization of the linear input polarization ($\varphi_0 \approx 90^\circ$ and $\approx \pm 45^\circ$ for the L and T cases) has to be easy to accomplish. The use of circularly polarized pump beams, making the beam coupling isotropic, also looks attractive for experiment; for the L case it should give an approximately two times smaller gain whereas for the T geometry the decreasing factor has to be much higher.

Antireflection coats are desirable for forward amplification experiments. In the absence of such coats, the opposite crystal faces could serve as a cavity for optical oscillation. Detection of an anomalously low threshold for such an oscillation can be considered as an alternative possibility for identification of the critical enhancement.

Above we have considered the dc technique for critical enhancement. Since the subharmonics can be generated under an ac field (with no frequency detuning), critical enhancement is expected also in this case. The theoretical description of this effect is more difficult as compared to the dc case because of the necessity to take into consideration the higher spatial harmonics, $2K, 3K$, etc. [37,38].

VII. CONCLUSIONS

We have developed a theory of the critical enhancement of the photorefractive response in cubic crystals by taking into account the real attributes of this phenomenon—the nonuniform broadening of the resonance owing to light absorption and the vectorial character of beam coupling. It is shown that despite the above complications there is a wide range of possibilities to achieve extremely high values of the spatial amplification in thin crystals by approaching from below the threshold of subharmonic generation. Our analytical and numerical results have allowed us to optimize the conditions for detection of the critical enhancement in BSO crystals and to predict its main observable features, including polarization, spectral, and orientation properties.

ACKNOWLEDGMENTS

Financial support from INTAS and Deutsche Forschungsgemeinschaft is gratefully acknowledged.

- [1] *Photorefractive Materials and Their Applications*, edited by P. Günther and J. P. Huignard, Vol. 1, Vol. 61 of *Topics in Applied Physics* (Springer-Verlag, Berlin, 1988); Vol. 2, Vol. 62 of *Topics in Applied Physics* (Springer-Verlag, Berlin, 1989).
- [2] L. Solymar, D. J. Webb, and A. Grunnet-Jepsen, *The Physics and Applications of Photorefractive Materials* (Clarendon

Press, Oxford, 1996).

- [3] M. P. Petrov, S. I. Stepanov, and A. V. Khomenko, *Photorefractive Crystals in Coherent Optical Systems* (Springer-Verlag, Berlin, 1991).
- [4] S. Mallik, B. Imbert, H. Ducollet, J. P. Herriau, and J. P. Huignard, *J. Appl. Phys.* **63**, 5660 (1988).

- [5] D. J. Webb and L. Solymar, *Opt. Commun.* **74**, 386 (1990).
- [6] D. J. Webb, L. B. Au, D. C. Jones, and L. Solymar, *Appl. Phys. Lett.* **57**, 1602 (1990).
- [7] J. Takacs, M. Schaub, and L. Solymar, *Opt. Commun.* **91**, 252 (1992).
- [8] I. Richter, A. Grunnet-Jepsen, J. Takacs, and L. Solymar, *IEEE J. Quantum Electron.* **30**, 1645 (1994).
- [9] K. Shcherbin, *Appl. Phys. B: Lasers Opt.* **71**, 123 (2000).
- [10] B. I. Sturman, A. Bledowski, J. Otten, and K. H. Ringhofer, *J. Opt. Soc. Am. B* **9**, 672 (1992).
- [11] B. I. Sturman, M. Mann, J. Otten, and K. H. Ringhofer, *J. Opt. Soc. Am. B* **10**, 1919 (1993).
- [12] O. P. Nestiorkin and Ye. P. Shershakov, *J. Opt. Soc. Am. B* **10**, 1907 (1993).
- [13] H. C. Pedersen and P. M. Johansen, *J. Opt. Soc. Am. B* **12**, 1065 (1995).
- [14] T. E. McClelland, D. J. Webb, B. I. Sturman, and K. H. Ringhofer, *Phys. Rev. Lett.* **73**, 3082 (1994).
- [15] B. I. Sturman, T. E. McClelland, D. J. Webb, E. Shamonina, and K. H. Ringhofer, *J. Opt. Soc. Am. B* **12**, 1621 (1995).
- [16] E. Serrano, M. Carrascosa, F. Agullo-Lopez, and L. Solymar, *Appl. Phys. Lett.* **64**, 658 (1994).
- [17] B. I. Sturman, A. I. Chernykh, E. Shamonina, V. P. Kamenov, and K. H. Ringhofer, *J. Opt. Soc. Am. B* **16**, 1099 (1999).
- [18] B. I. Sturman, M. Aguilar, F. Agullo-Lopez, and K. H. Ringhofer, *Phys. Rev. E* **55**, 6072 (1997).
- [19] E. V. Podivilov, H. C. Pedersen, P. M. Johansen, and B. I. Sturman, *Phys. Rev. E* **57**, 6112 (1998).
- [20] H. C. Pedersen and P. M. Johansen, *Phys. Rev. Lett.* **77**, 3106 (1996).
- [21] S. F. Lyusyutov, P. Buchave, and M. Vasnetsov, *Phys. Rev. Lett.* **79**, 67 (1997).
- [22] E. V. Podivilov, B. I. Sturman, H. C. Pedersen, and P. M. Johansen, *Phys. Rev. Lett.* **85**, 1867 (2000).
- [23] K. H. Ringhofer and L. Solymar, *Appl. Phys. Lett.* **53**, 1039 (1988).
- [24] K. H. Ringhofer and L. Solymar, *Appl. Phys. B: Photophys. Laser Chem.* **48**, 395 (1989).
- [25] D. J. Webb and L. Solymar, *Opt. Commun.* **83**, 287 (1991).
- [26] B. I. Sturman, A. I. Chernykh, V. P. Kamenov, E. Shamonina, and K. H. Ringhofer, *J. Opt. Soc. Am. B* **17**, 985 (2000).
- [27] A. Marrakchi, R. V. Johnson, and A. R. Tanguay, *J. Opt. Soc. Am. B* **3**, 321 (1986).
- [28] B. I. Sturman, E. V. Podivilov, K. H. Ringhofer, E. Shamonina, V. P. Kamenov, E. Nippolainen, V. V. Prokofiev, and A. A. Kamshilin, *Phys. Rev. E* **60**, 3332 (1999).
- [29] L. D. Landau and E. M. Lifshiz, *Quantum Mechanics* (Pergamon Press, Oxford, 1969).
- [30] B. I. Sturman, D. J. Webb, R. Kowarschik, E. Shamonina, and K. H. Ringhofer, *J. Opt. Soc. Am. B* **11**, 1813 (1994).
- [31] V. P. Kamenov, Y. Hu, E. Shamonina, K. H. Ringhofer, and V. Y. Gayvoronsky, *Phys. Rev. E* **62**, 2863 (2000).
- [32] V. V. Shepelevich, S. M. Shandarov, and A. E. Mendel, *Ferroelectrics* **110**, 235 (1990).
- [33] G. Pauliat, P. Mathey, and G. Roosen, *J. Opt. Soc. Am. B* **8**, 1942 (1991).
- [34] L. D. Landau and E. M. Lifshitz, *Field Theory* (Pergamon Press, Oxford, 1969).
- [35] H. C. Pedersen, P. M. Johansen, and D. J. Webb, *J. Opt. Soc. Am. B* **15**, 1528 (1998).
- [36] H. C. Pedersen, D. J. Webb, and P. M. Johansen, *J. Opt. Soc. Am. B* **15**, 2439 (1998).
- [37] G. A. Brost, *J. Opt. Soc. Am. B* **9**, 1454 (1992).
- [38] P. M. Johansen, H. C. Pedersen, E. V. Podivilov, and B. I. Sturman, *Phys. Rev. A* **58**, 1601 (1998).